A 3D multi-mode geometry-independent RMP optimization method and its application to TCV

J X Rossel, J-M Moret, Y Martin and the TCV team [1]

Ecole Polytechnique Fédérale de Lausanne (EPFL)
Centre de Recherches en Physique des Plasmas
Association Euratom Confédération Suisse
CH-1015 Lausanne, Switzerland

E-mail: jonathan.rossel@epfl.ch

Abstract.

Resonant magnetic perturbation (RMP) and error field correction produced by toroidally and poloidally distributed coil systems can be optimized if each coil is powered with an independent power supply. A 3D multi-mode geometry-independent Lagrange method has been developed and appears to be an efficient way to minimize the parasitic spatial modes of the magnetic perturbation and the coil current requirements while imposing the amplitude and phase of a number of target modes. A figure of merit measuring the quality of a perturbation spectrum with respect to RMP independently of the considered coil system or plasma equilibrium is proposed. To ease the application of the Lagrange method, a spectral characterization of the system, based on a generalized discrete Fourier transform applied in current space, is performed to determine how spectral degeneracy and side-bands creation limit the set of simultaneously controllable target modes. This characterization is also useful to quantify the efficiency of the coil system in each toroidal mode number and to know whether optimization is possible for a given number of target modes.

The efficiency of the method is demonstrated in the special case of a multi-purpose saddle coil system proposed as part of a future upgrade of TCV. This system consists of 3 rows of 8 internal coils, each coil having independent power supplies, and provides simultaneously error field correction, RMP and fast vertical position control.

PACS numbers: 52.25.Gj, 52.25.Xz, 52.30.Cv, 52.35.Vd, 52.55.Fa, 52.55.Rk, 52.55.Wq, 28.52.Av

Submitted to: *Plasma Phys. Control. Fusion*

1. Introduction

Edge localized modes (**ELM**) [2], related to the high confinement regime (H-mode) [3], lead to a degradation of the plasma confinement and a release of energetic particles towards the vessel walls. Scaling the current experimental data to ITER predicts that the power flux related to type-I ELMs will cause an intolerable erosion and heat load on the plasma facing components [4, 5]. Experiments on DIII-D [6, 7] and JET [8] have demonstrated that the application of resonant magnetic perturbation (**RMP**) is able to mitigate or suppress ELMs while keeping sufficient confinement properties. The current explanation of this phenomenon is based on the overlap of the magnetic islands created by the RMP that generates an ergodic zone in the plasma edge, itself increasing the outward transport and thereby limiting the pedestal gradients to values below the instability limits. This description is however still incomplete as the weak effect of RMP on the pedestal electron temperature remains unexplained. The limits of the process, in terms of operation domain, are not yet accurately known, DIII-D being up to now the only Tokamak where a complete suppression of type-I ELMs has been successfully obtained. In addition, experiments in different Tokamaks reveal opposite results for similar conditions, for example RMP can trigger ELMs during ELM-free phases in COMPASS [9], NSTX [10] and MAST [11]. While a mitigation of type-IV ELMs has been achieved with external error field correction coils on MAST [11, 12], the dedicated set of internal coils has not been able to mitigate type-I ELMs up to now, even though the criterion of edge ergodization was satisfied. With that respect, TCV (Tokamak à Configuration Variable) unique plasma shaping and positioning capability could extend the range of accessible magnetic perturbation schemes for a given RMP coil system geometry and contribute to a clearer description of the conditions required for ELM suppression.

When applying asymmetric magnetic perturbations to generate RMP, the spectrum of the perturbation should be optimized for what is thought to be efficient for ELM mitigation [13, 14]: (a) minimal resonant mode amplitude in the core to avoid triggering of MHD instabilities, (b) maximal resonant mode amplitude near the edge to obtain the ergodization of the edge region, (c) minimal non resonant mode amplitude to avoid parasitic effects such as plasma braking or acceleration due to neoclassical toroidal viscosity [15–17] and (d) no or minimal side-band modes to avoid parasitic effects that could impair the interpretation of the experimental results. All these aspects justify the development of the optimization method presented in this paper.

Error fields are another aspect of toroidally asymmetric magnetic fields. They are due to construction tolerances in Tokamak coil positions and shapes. These fields, dominated by low values of the toroidal mode number, induce plasma braking and locked modes [18], themselves responsible for disruptions. Their effects can be corrected by applying an asymmetric field of opposite sign. Despite the distinction generally present in the literature, error field correction (**EFC**) and RMP are strongly related, since they both rely on effects due to the component of a non axisymmetric perturbation

magnetic field perpendicular to the flux surfaces. In the case of EFC, both non resonant and resonant perturbations are present. In the case of RMP, the focus is on resonant perturbation, but non resonant ones generally dominates in amplitude. Both concept can and should therefore be studied with the same set of tools.

When error field correction coils or RMP coil systems are fed with independent power supplies, the effectiveness of the created perturbation may be enhanced by a fine tuning of the relative distribution of currents in the coils. Hanson [19, 20] has developed a method of optimization of the correction coil currents based on a least square approach and working with Fourier components in the current space, consequently limited to evenly spaced coil systems. We present here (section 2) a method of optimization of the currents of generic radial field coil systems based on Lagrange multipliers, working in real current space. This method is not limited to evenly spaced identical coil systems and allows simultaneous multi-mode optimization. It would therefore also apply if one of the coils becomes unavailable. Using a Lagrange method allows to distinguish between constraints to satisfy exactly – e.g. the corrected error field – and optimization of cost functions – e.g. the minimization of core islands in the case of ELM mitigation. We show (section 2.4) that the Lagrange method is an efficient way to minimize parasitic modes and current requirements while imposing the amplitude and phase of a number of target modes. For example, the relative amplitude of edge modes can be increased at the cost of lower absolute amplitudes, demonstrating a degree of controllability on the localization of the magnetic perturbation. In this process, a figure of merit may be used to quantify the optimization of the magnetic spectrum. Section 2.3 shows how the Lagrange method is used to maximize such a figure of merit. The dependence of the figure of merit on the value of the edge safety factor and the robustness of an optimal current distribution with respect to a change in the plasma equilibrium are analysed in section 2.5. Finally, linear optimization methods, as the least square or Lagrange ones, cannot directly minimize the maximal current required in the coil set but rather the norm of the vector made of all the coil currents. The implications of this simplification are described in section 2.2 and a workaround is given. We show that in some cases, up to 40% of mode amplitude can be gained for the same maximal coil current (section 3.3).

The characterization of a coil system in terms of spectral degeneracy, number of simultaneously controllable target modes, availability of optimization for a given number of target modes and efficiency in each toroidal mode is crucial in order to apply the Lagrange method. The study presented in section 3 describes a simple method to obtain such a characterization, using a generalized discrete Fourier transform.

The Lagrange method is illustrated in the special case of a multi-purpose saddle coil system (**SCS**) proposed as part of a future upgrade of TCV (figure 1 and section 4). This system consists of 3 rows of 8 internal coils, each coil having independent power supplies, and provides simultaneously EFC, RMP and fast vertical position control (**VC**). Other applications, like resistive wall mode control and controlled plasma rotation, are also considered for this system. The technical aspects of this upgrade will be presented in a future publication.

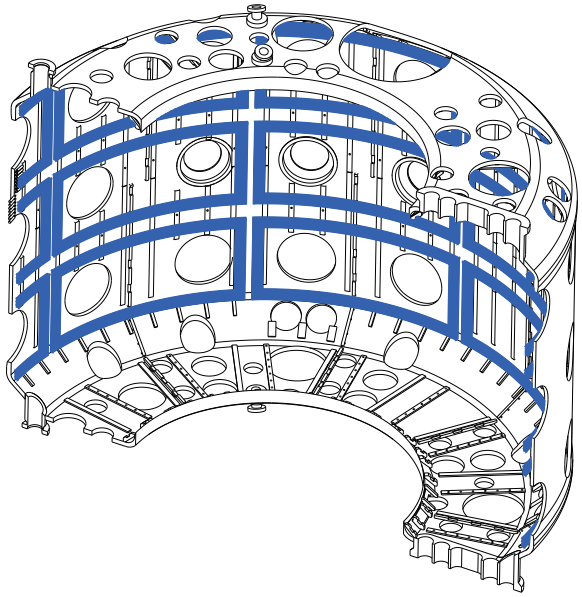

Figure 1. Perspective view of the TCV saddle coil system project (in blue), drawn on top of the vacuum vessel (in black). The system consists of 3 rows of 8 internal saddle coils located on the low field side of the torus.

2. Optimization method

RMP is related to the calculation of magnetic islands generated on resonant flux surfaces by $B_\perp$, the component of the perturbation magnetic field perpendicular to the flux surfaces. An analytical derivation of the width of the islands is given in [19, 20] for non circular Tokamak plasmas. We express it here in a form consistent with [21]. The straight field line coordinates (ρ, θ^*, ϕ) [22] are used to describe the perturbation: $\rho = \sqrt{\psi_{01}}$ is the normalized radius (ψ_{01} being the normalized poloidal flux), ϕ the toroidal angle and $\theta^*(\rho, \theta)$ is such that the equilibrium field $\boldsymbol{B}_0$ follows straight lines in a (θ^*, ϕ)-plane. The Biot-Savart law is used to calculate the vacuum perturbation magnetic field due to the SCS in 3-D. The various coordinate transformations and vector projections are performed in the framework of the ψ-toolbox [22]. The width of the islands is then given by:

$$\Delta\rho_s = 4\sqrt{\frac{2|\tilde{b}(\rho_s, m, n)|q_s^2}{|mq_s'|}} \tag{1}$$

with m the poloidal mode number, n the toroidal mode number, s the resonant flux surface index, $q' = \mathrm{d}q/\mathrm{d}\rho$ the radial derivative of the safety factor q and $\tilde{b}$ the space Fourier transform of b:

$$\tilde{b}(\rho, m, n) = \frac{1}{(2\pi)^2} \iint_0^{2\pi} \mathrm{d}\phi \mathrm{d}\theta^* b(\rho, \theta^*, \phi) \mathrm{e}^{\mathrm{i}(-m\theta^* - n\phi)} \tag{2}$$

with b the locally normalized perpendicular vacuum magnetic perturbation due to the coil system:

$$b(\rho, \theta^*, \phi) = \frac{B_\perp R \|\nabla \rho\|}{B_{0,\phi}} \tag{3}$$

with R the major radius coordinate and $B_{0,\phi}$ the toroidal component of the equilibrium magnetic field. The Chirikov parameter σ used to characterize the degree of overlapping of magnetic islands is defined by:

$$\sigma_{s+1/2} = \frac{\Delta\rho_s + \Delta\rho_{s+1}}{2(\rho_{s+1} - \rho_s)} \tag{4}$$

The criterion of ergodization is given by $\sigma_{s+1/2} \geq 1$. Equations (1) and (4) show that $|\tilde{b}|$ is the parameter of interest for studying the efficiency of a given magnetic perturbation.

The cost function f minimized in the Lagrange approach is defined as a linear combination of the current cost function f_{cur} and the cost functions f_k related to sets of optimized modes S_k:

$$f(\{I_c\}) = f_{cur}(\{I_c\}) + \sum_k w_k f_k(\{I_c\}) \tag{5}$$

with I_c the coil currents. The weight on f_{cur} is used as reference and is set to 1. w_k are relative weights, with $w_k > 0$ (resp. $w_k < 0$) for a minimization (resp. maximization) of f_k. f_k and their normalization factors N_k are defined by:

$$f_k = \frac{1}{N_k} \sum_{p \in S_k} \left[\left(\sum_c \tilde{b}_{cp,r} I_c - \Re(a_p e^{i\alpha_p}) \right)^2 + \left(\sum_c \tilde{b}_{cp,i} I_c - \Im(a_p e^{i\alpha_p}) \right)^2 \right] \tag{6}$$

$$N_k = \sum_{p \in S_k} A_p^2 \tag{7}$$

$$A_p = \left[\left(\sum_c |\tilde{b}_{cp,r}| \right)^2 + \left(\sum_c |\tilde{b}_{cp,i}| \right)^2 \right]^{1/2} \tag{8}$$

with p the index on modes defined by (ρ, m, n), $\tilde{b}_{cp,r}$ (resp. $\tilde{b}_{cp,i}$) the real (resp. imaginary) part of mode p due to coil c and $a_p e^{i\alpha_p}$ the target value to be approached for mode p, with amplitude a_p and phase α_p. A_p is a measure of the natural distribution of the amplitude of the modes created by the SCS. Note that even though maximization of f_k is possible when using a negative weight, f, as a quadratic form, must remain positive definite to ensure that its constrained extremum is neither a maximum nor a saddle point. Consequently, a negative weight should always be chosen so that the maximized cost function does not dominate the overall cost.

The exact target modes, i.e. the constraints of the Lagrange method, are a set of chosen modes whose amplitudes a_t and phases α_t must be exactly generated by the coil system. They are introduced by defining:

$$g_{t,r}(\{I_c\}) = \sum_c \tilde{b}_{ct,r} I_c - \Re(a_t e^{i\alpha_t}) \tag{9}$$

$$g_{t,i}(\{I_c\}) = \sum_c \tilde{b}_{ct,i} I_c - \Im(a_t e^{i\alpha_t}) \tag{10}$$

with t the index of the target mode. The constraints are fulfilled if:

$$g_{t,r}(\{I_c\}) = 0 \qquad g_{t,i}(\{I_c\}) = 0 \qquad \forall t \tag{11}$$

Note that the constraint part depends linearly on the currents. If the phases of the approximative or exact target modes are free parameters, the phase combination leading to the lowest total cost f is selected.

Finally, the Lagrange method requires an auxiliary function h defined by:

$$h(\{I_c\}, \{\lambda_t\}) = f(\{I_c\}) + \sum_t \left[\lambda_{t,r} g_{t,r}(\{I_c\}) + \lambda_{t,i} g_{t,i}(\{I_c\})\right] \tag{12}$$

with Lagrange multipliers λ_t. The constrained optimum is found by solving:

$$\nabla_{\{I_c\},\{\lambda_t\}} h = 0 \tag{13}$$

The solution must then be checked to be a minimum. A simple approach consists in exploring the affine sub-space of solutions around the optimal coil current vector $\boldsymbol{I}_{opt}$. Defining:

$$\mathbf{C} = \begin{pmatrix} \begin{pmatrix} \tilde{b}_{ct,r} \end{pmatrix} \\ \begin{pmatrix} \tilde{b}_{ct,i} \end{pmatrix} \end{pmatrix}, \tag{14}$$

the coil current vectors fulfilling the constraints are given by: $\boldsymbol{K} + \boldsymbol{I}_{opt}$ where $\boldsymbol{K} \in \ker(\mathbf{C})$, the null space of $\mathbf{C}$. $\boldsymbol{I}_{opt}$ is a minimum of f if $f(\boldsymbol{I}_{test}) > f(\boldsymbol{I}_{opt})$ for any $\boldsymbol{I}_{test} = \boldsymbol{I}_{opt} \pm \epsilon \|\boldsymbol{I}_{opt}\| \boldsymbol{k}_i$ where $\boldsymbol{k}_i$ is the i-th basis vector of $\ker(\mathbf{C})$ and ϵ is small.

If some of the coils have a fixed connection, their magnetic field must be combined prior to the application of the optimization method. The subset of coils should then appear as a single equivalent coil within the method.

2.1. Linear approach

In the linear approach, $\nabla_{\{I_c\}} f$ must be a linear combination of the coil currents. The current cost function is therefore defined as:

$$f_{cur} = \frac{1}{N_{coils}} \sum_c I_c^2 \tag{15}$$

where N_{coils} is the total number of coils. In this case, solving (13) is equivalent to inverting a full rank linear system of equations.

2.2. Non linear approach

The linear method presented in section 2.1 minimizes the norm of the current vector, a simplified version of the non linear real technical constraint $\max_c(|I_c|)$. A non linear algorithm has been created to minimize f_{nl}, the non linear cost given by using $\max_c(I_c^2)$ instead of $\sum_c (I_c)^2$ in f. It is based on the exploration of the affine space of currents fulfilling the constraints, starting from the solution provided by the linear approach. It calculates the cost in each orthogonal directions and moves to the combination of directions minimizing the cost. Note that when using the non linear cost for evenly

spaced coil systems, side-band modes must be introduced in the cost function to force their minimization.

If the target mode phases are free parameters, an effective approach consists in using the linear solution for each phase combination, but using the non linear cost to select the optimal phase combination. This approach has been retained as the standard resolution method.

2.3. Maximization of a figure of merit

The choice of the set of weights w_k in (5) is usually driven by physical requirements: low currents or high relative amplitude of a certain region of the magnetic spectrum. In certain cases, the requirements can be summarized by a figure of merit, qualifying to which extent these requirements are met. In some ways, this approach replaces the arbitrary choice of weights by an arbitrary definition of a figure of merit.

In the case of RMP, the spectrum of b must be optimized to obtain minimal resonant core mode amplitudes, maximal edge ergodization and minimal non resonant mode amplitudes. These conditions are satisfied with an approach based on two sets of modes: the first set, S_e, consists of the resonant edge modes. The second set, S_g, includes all the modes of the spectrum. Formally, S_e and S_g are written:

$$S_e = \{(\rho, m, n) \mid \rho_{lim} \leq \rho \leq \rho_{95},\ q(\rho) = m/n,\ n = n_t\} \tag{16}$$

$$S_g = \{(\rho, m, n) \mid \rho \leq \rho_{95},\ -20 \leq m \leq 20,\ n = n_t\} \tag{17}$$

with n_t the target value of n and ρ_{lim} the inner radius of the selected ergodized zone. The interval $[-20, 20]$ appearing in S_d is chosen as integration boundaries since the mode amplitudes outside this interval are negligible. $\rho_{95} = \sqrt{0.95}$ is used as an upper limit to avoid the singularity due to the X-point at the last closed flux surface. The optimization of the edge modes is based on the Chirikov criterion. By analogy with (4), the separate contribution of each mode to the Chirikov parameter may be defined as $C_s = \Delta\rho_s/(\rho_{s+1} - \rho_{s-1})$, with an equivalent approximative ergodization criterion given by $C_s = 1/2$. Using (1), the minimal mode amplitudes required to fulfill the ergodization of the edge are then given by:

$$a_e = \frac{|mq'_e|(\rho_{e+1} - \rho_{e-1})^2}{128 q_e^2} \tag{18}$$

A possible definition for a figure of merit r quantifying the quality of a spectrum with respect to RMP is given below:

$$r = \left[\frac{|\tilde{b}_{e_{max}}|^2}{\left(1 + \max_{|\tilde{b}_e| < a_e} \left\{ \left((|\tilde{b}_e| - a_e)/a_e \right)^2 \right\} \right) \int_{S_g} |\tilde{b}|^2 \mathrm{d}\rho} \right]^{1/2} \tag{19}$$

with e_{max} the index of the resonant edge mode having the highest a_e. The main term in (19) is the ratio between the amplitude of the maximal edge mode and the integral of the spectrum. This ratio increases as $|\tilde{b}_{e_{max}}|$ becomes relatively larger

and as the spectrum becomes more peaked, so that an increase in r does reflect an increase of quality of the spectrum, as defined in the frame of RMP. The factor $\left(1+\max_{|\tilde{b}_e|<a_e}\left\{\left((|\tilde{b}_e|-a_e)/a_e\right)^2\right\}\right)$ in r is a correction factor which impairs the figure of merit if one of the resonant edge modes has an amplitude lower than the minimal amplitude required for ergodization. The normalization by a_e in this correction factor comes from the expression of C_s, when written as a function of a_e: $C_e=\sqrt{|\tilde{b}_e|/(4a_e)}$.

The link between r and the optimization method is established by associating two cost functions as defined in (6) to both the main term and the correction factor in r, respectively f_g and f_e, and by using e_{max} as unique exact target mode. The total cost function f is defined here as:

$$f_{RMP}(\{I_c\})=f_{cur}(\{I_c\})+w_e f_e(\{I_c\})+w_g f_g(\{I_c\}) \tag{20}$$

f_e acts on modes included in S_e with approximate target amplitudes given by (18) and f_g acts on modes included in S_g with null target amplitudes ($a_g=0$). f_e is active only on the subset of resonant edge modes having $|\tilde{b}_e|<a_e$ to avoid an unnecessary and detrimental flattening of the Chirikov parameter in the edge. In addition, a cross-mode normalization is necessary in f_e to minimize the relative distance to a_e instead of the absolute one, consistently with the expression of C_e given above. Formally, f_e is written as:

$$f_e=\frac{1}{N_e}\sum_{p\in S_e^{sub}}\frac{1}{a_p^2}\left[\left(\sum_c \tilde{b}_{cp,r}I_c-\Re(a_p\mathrm{e}^{\mathrm{i}\alpha_p})\right)^2+\left(\sum_c \tilde{b}_{cp,i}I_c-\Im(a_p\mathrm{e}^{\mathrm{i}\alpha_p})\right)^2\right] \tag{21}$$

$$N_e=\sum_{p\in S_e^{sub}}\frac{A_p^2}{a_p^2} \tag{22}$$

where $S_e^{sub}=\{p\in S_e \mid |\tilde{b}_p|<a_p\}$.

The optimization of r is obtained by iteratively calculating $r(w_g,w_e)$. When increasing w_g, the integral of the spectrum decreases whereas $|\tilde{b}_{e_{max}}|$ remains constant, therefore increasing r. In this process, if modes with $|\tilde{b}_e|<a_e$ are detected, f_e is activated on this subset of weak modes to limit their negative impact on r.

The approach described above has several advantages: (a) the iterative process of weight selection to optimize r is at most bidimensional, independently of the considered coil system; (b) the minimization of the coil current is included in f_{RMP}, allowing a direct estimation of the gain in r with respect to the increase in required current; (c) both f_e and f_g are minimized in the proposed process, which means that the existence of a global minimum of f_{RMP} is always guaranteed; (d) the definition of r proposed in (19) involves only normalized or relative quantities and is therefore a good candidate to measure the adequacy of a coil system for a range of magnetic equilibria.

2.4. Optimization method results

In the case of RMP, the toroidal modes of interest for the TCV SCS are $n = 2$, $n = 3$ and $n = 4$. The results presented here are obtained for a standard diverted H-mode plasma located on the midplane of the machine and characterized by a density on axis $n_e = 7.5 \cdot 10^{19}\,\mathrm{m}^3$, a plasma current $I_p = 415\,\mathrm{kA}$, a toroidal magnetic field on axis $B_{\phi,axis} = 1.4\,\mathrm{T}$, a major radius $R_{axis} = 0.91\,\mathrm{m}$, a minor radius $a = 0.22\,\mathrm{m}$, a triangularity $\delta_{95} = 0.4$, an elongation $\kappa_{95} = 1.7$, a normalized pressure $\beta_p = 0.65$ and a safety factor $q_{95} = 2.6$. As described by Fenstermacher [23], an ergodization width of $\Delta\psi_{01} = 0.17$ of the plasma edge is sufficient to obtain type I ELM suppression on DIII-D. This is equivalent to setting the ergodized zone limit at $\rho_{lim} = 0.911$.

Figure 2 (solid lines) shows the figure of merit r as a function of the weight w_g for the different values of n_t. The maximum of r has an asymptotic character. This feature is inherent to the method since the current distribution converges to a fixed distribution as the f_e and f_g terms dominate in f_{RMP}, leading to a saturation of r. The asymptotic value will be referred to as the optimal r in the remainder of this paper. The experimental equilibrium used for the calculation of r shown in figure 2 does not require the activation of f_e because the resonant edge modes stay at amplitudes above the Chirikov criterion for all values of w_g. A synthetic case requiring the activation of f_e is presented in figure 3. The same saturation mechanism occurs, but its location now depends on the ratio of w_e and w_g. Due to the very small gradient of r around its asymptotic maximum, any set of weights chosen in this area can be considered as satisfactory.

The minimal coil current I_{req} required to obtain an ergodization of the edge down to ρ_{lim} is a parameter complementary to r, as it reveals whether the optimal r configuration is technically feasible. The calculation of this current is based on the Chirikov criterion. At ρ_{lim}, a sufficient condition is that the first edge island ($\rho > \rho_{lim}$) overlaps either ρ_{lim} or the last core island ($\rho < \rho_{lim}$). The minimal I_{req} is then determined from (1). Figure 2 (dashed-dotted lines) shows I_{req} as a function of w_g. As expected, the lowest current is obtained when w_g is close to zero. The slight offset in the location of the minimum of the current, observable for $n_t = 2$ and $n_t = 3$, is a consequence of the semi-linear approach used to define the current cost function f_{cur}, as described in section 2.2: minimizing the norm of the current vector does not guarantee to obtain the lowest maximal current. Figure 2 also shows that I_{req} remains within acceptable values when r is optimal. It must be noted that the edge ergodization criterion is satisfied at much lower currents if larger non resonant components are allowed, leaving some margin on the coil current requirement.

In order to assess the efficiency of the method on magnetic spectra, two different sets of weights are used. In the first case, only the current minimization is present. This corresponds to the set of weights $(w_e, w_g) = (0, 0)$. In the second case, a set of weights giving an optimal figure of merit r is determined using figure 2. Since r is independent of w_e here, the set $(w_e, w_g) = (0, 10^5)$ is used in all cases. The current

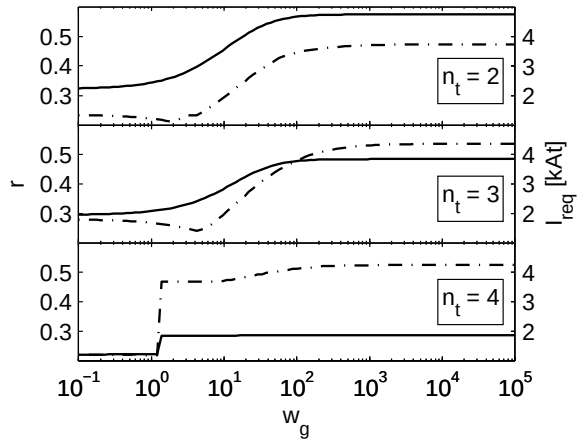

Figure 2. Figure of merit r (solid lines) and required current for edge ergodization I_{req} (dashed-dotted lines) as a function of the weight w_g in the cases $n_t = 2$, $n_t = 3$ and $n_t = 4$. For these cases, r is independent of w_e.

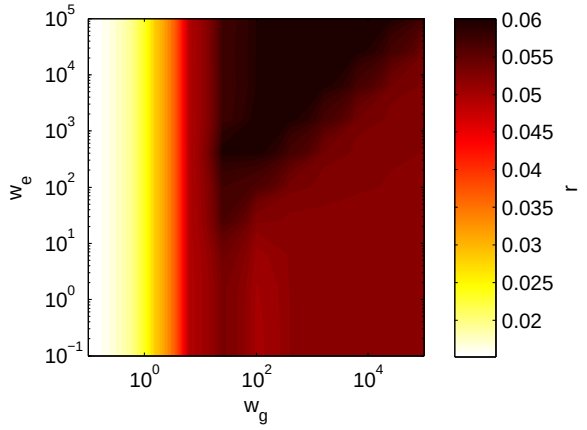

Figure 3. Figure of merit r as a function of the weights for a synthetic equilibrium case ($n_t = 3$, $q_{95} = 8.3$). The dependence of r on w_e appears for $w_g > 20$.

distributions corresponding to both $n_t = 2$ cases are displayed in figures 4 and 5. In the case where r is optimized, the bottom and top rows of coils, less efficient in terms of magnetic perturbation amplitudes, have much stronger contributions. This behaviour is consistent with the optimization of r, which shapes the perturbation spectrum using all the available degrees of freedom, without taking the current consumption into consideration. Figures 6 to 11 show $|\tilde{b}|$ for the different values of n_t. In each case, a maximal coil current of 1 At is used to ease the comparison of the perturbation amplitudes. For each toroidal mode number target, the method proves its efficiency at either minimizing the currents (observed here by a higher absolute amplitude of the modes) or optimizing the spectrum, i.e. increasing the relative amplitude of the resonant edge modes. For $n_t = 3$ (figure 9), the optimization of the spectrum has the side effect of increasing the relative amplitude of non resonant modes. This reveals that despite

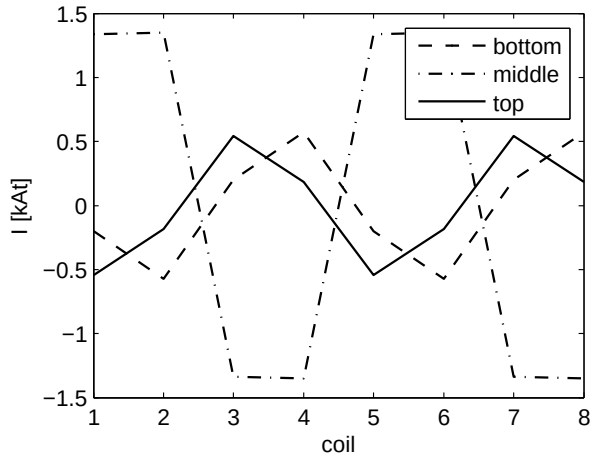

Figure 4. Current distributions of the 3 coil rows of the TCV SCS for a $n_t = 2$ target and a set of weights minimizing the current amplitude: $(w_e, w_g) = (0, 0)$ (see figure 2). The current distribution is scaled to satisfy the condition of edge ergodization: $I_{req} = 1.4\,\mathrm{kAt}$. $r = 0.32$.

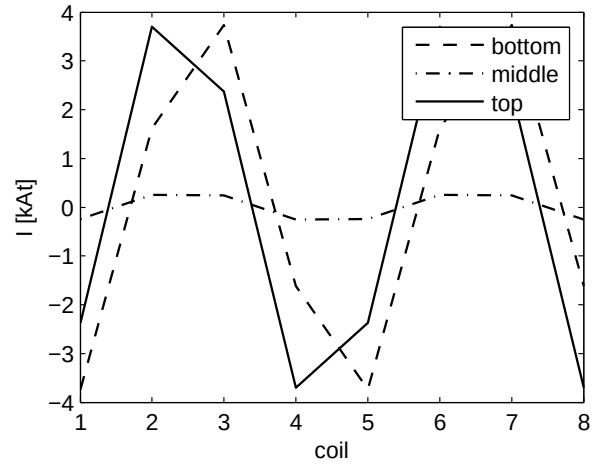

Figure 5. Current distributions of the 3 coil rows of the TCV SCS for a $n_t = 2$ target and a set of weights optimizing the figure of merit r: $(w_e, w_g) = (0, 10^5)$ (see figure 2). The current distribution is scaled to satisfy the condition of edge ergodization: $I_{req} = 3.7\,\mathrm{kAt}$. $r = 0.57$.

the clear advantage of using the optimization method, the low number of degrees of freedom imposes limits on the process. Even though $n = 3$ is not a natural mode of the coil system, the edge mode amplitudes are comparable to those of $n_t = 2$ (figure 7), proving the flexibility of the system and allowing this configuration for experimental studies. It should also be noted that the obtained perturbation is a pure $n = 3$ mode, within the limit of the degeneracy described in section 3.

The case $n_t = 4$ (figures 10 and 11) is a special case for the considered coil system as it corresponds to $N_s/2$ where N_s is the number of coils per row. In this case, the

system has a higher order of symmetry ($b(-\phi) = b(\phi)$) which results in a symmetrical spectrum with respect to $m = 0$, as well as a lower number of degrees of freedom for the optimization. Using a higher value of n has two downsides in terms of RMP: first the activated edge modes have a lower amplitude since the values of m required for the same value of q are higher, second the width of the islands is smaller due to the factor m in (1). However, in the case $n_t = N_s/2$, each coil of a row is powered with the same current, resulting in a stronger perturbation than for the other cases, and the number of resonant flux surfaces, therefore the number of islands, is also larger. Altogether, these effects compensate each other and result in good performances of the system for $n_t = 4$, as shown in figure 12. Such a configuration is also interesting as the corresponding degenerate modes are extremely weak (see section 3).

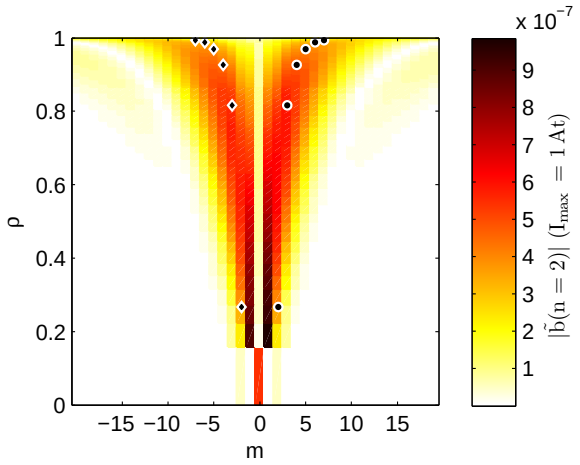

Figure 6. $\left|\tilde{b}(\rho, m, n = 2)\right|$. Target: $n_t = 2$ outside $\rho_{lim} = 0.911$. Minimized current amplitude: $(w_e, w_g) = (0, 0)$. $I_{req} = 1.4\,\text{kAt}$ and $r = 0.32$ (see figure 2). ● : resonant flux surfaces location, ♦: symmetrical non resonant counterparts.

2.5. Edge safety factor dependence and robustness analysis

The results shown in section 2.4 have all been generated with the same experimental equilibrium. It is of interest to study how the optimal figure of merit and its related required current evolve with respect to a change in the magnetic equilibrium, since such a study contributes to the assessment of the adequacy of a RMP coil system. Amongst the different equilibrium parameters that impact the effects of a coil system, q_{95} is certainly the most important one since it drives the requirements for the spectral location of the magnetic perturbation and consequently has a strong influence on r and I_{req}. For this study, a series of synthetic equilibria generated with the free boundary code FBTE [24] are used to simulate a scan on q_{95} while keeping other parameters as constant as possible. These equilibria are characterized by: $q_{95} \in [2.0, 8.3]$, $q_{axis} = 0.8$, $I_p \in [575, 125]\,\text{kA}$, $\beta_p = 0.36$, $\delta_{95} \in [0.42, 0.30]$, $\kappa_{95} \in [1.70, 1.58]$, $B_{\phi,axis} = 1.4\,\text{T}$, $R_{axis} = 0.89\,\text{m}$ and $a = 0.23\,\text{m}$.

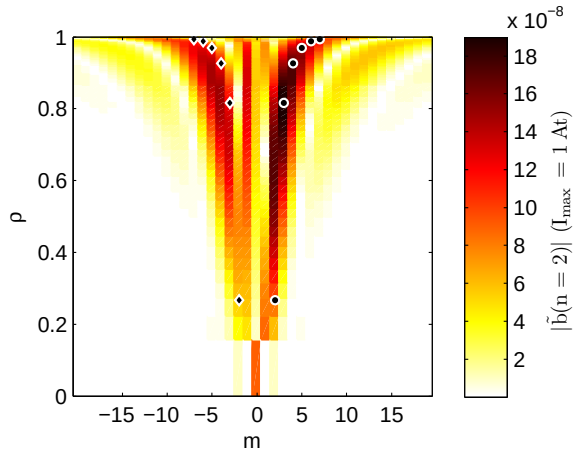

Figure 7. $\left|\tilde{b}(\rho, m, n = 2)\right|$. Target: $n_t = 2$ outside $\rho_{lim} = 0.911$. Optimized figure of merit r: $(w_e, w_g) = (0, 10^5)$. $I_{req} = 3.7\,\mathrm{kAt}$ and $r = 0.57$ (see figure 2).

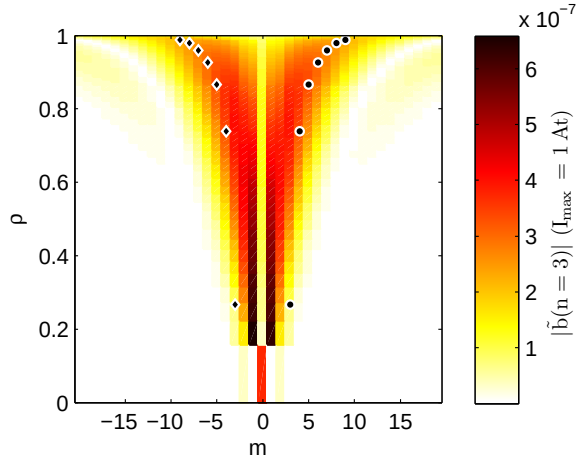

Figure 8. $\left|\tilde{b}(\rho, m, n = 3)\right|$. Target: $n_t = 3$ outside $\rho_{lim} = 0.911$. Minimized current amplitude: $(w_e, w_g) = (0, 0)$. $I_{req} = 1.8\,\mathrm{kAt}$ and $r = 0.30$ (see figure 2).

The solid lines on figures 13 and 14 show the optimal figure of merit r_{opt} as a function of q_{95} and the corresponding I_{req}. The main trend of $r_{opt}(q_{95})$ is its decrease as q_{95} or n_t increases, consistently with the naturally low amplitude of higher m modes. The small undulations of r_{opt} along q_{95} are due to the regular crossing of higher amplitude ridges naturally appearing in the spectra (see figures 7, 9 and 11) as the locus of resonant surfaces moves to higher values of m. $I_{req}(q_{95}, r_{opt})$ displays different behaviours as q_{95} increases. At low q_{95}, I_{req} displays oscillations whose amplitudes decrease with n_t and q_{95}. For these values of q_{95}, I_{req} is always determined by the first edge island and the oscillations are hence due to variations in the distance between the ergodized region limit ρ_{lim} and the first island position. These oscillations decrease in amplitude as the number of islands in the edge increases, consistently with increasing n_t or q_{95}. At higher

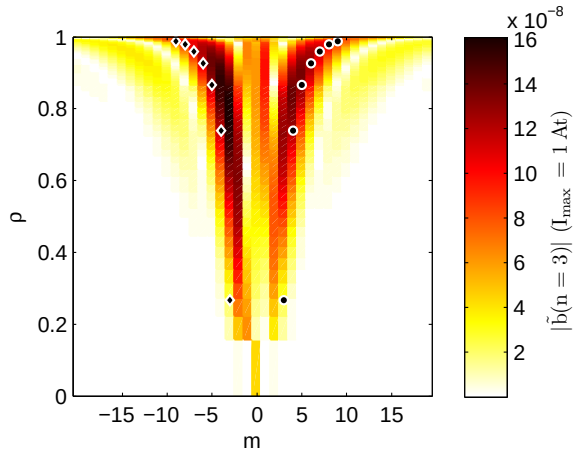

Figure 9. $\left|\tilde{b}(\rho, m, n = 3)\right|$. Target: $n_t = 3$ outside $\rho_{lim} = 0.911$. Optimized figure of merit r: $(w_e, w_g) = (0, 10^5)$. $I_{req} = 4.4\,\mathrm{kAt}$ and $r = 0.48$ (see figure 2).

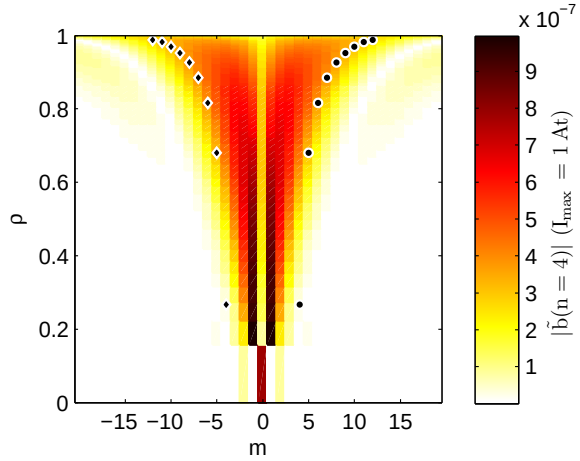

Figure 10. $\left|\tilde{b}(\rho, m, n = 4)\right|$. Target: $n_t = 4$ outside $\rho_{lim} = 0.911$. Minimized current amplitude: $(w_e, w_g) = (0, 0)$. $I_{req} = 1.2\,\mathrm{kAt}$ and $r = 0.22$ (see figure 2).

q_{95}, I_{req} may present some discontinuities. They typically occur when the q profile passes over an inter-ridge spectral zone within the edge region, therefore leading to a large required current in order to satisfy the ergodization constraint. When filtering out the low q_{95} oscillations and the high q_{95} discontinuities, I_{req} displays a global minimum at $q_{95} \sim 7$ for $n_t = 2$, at $q_{95} \sim 4.5$ for $n_t = 3$ and at $q_{95} \sim 3.5$ for $n_t = 4$. This reflects a trade-off between the number of islands, increasing with q_{95}, and the size of the islands, decreasing with q_{95}. In terms of RMP coil system qualification, the obtained results show that $I_{req}(q_{95}, r_{opt})$ remains within reasonable range in the typical operational interval of $q_{95} \in [2, 6]$. Of course, lower I_{req} are possible if an optimal r is not required. The decrease of r_{opt} when the resonant edge modes have high values of m could only be counteracted by a modification of the SCS design, for example by increasing the number of rows and

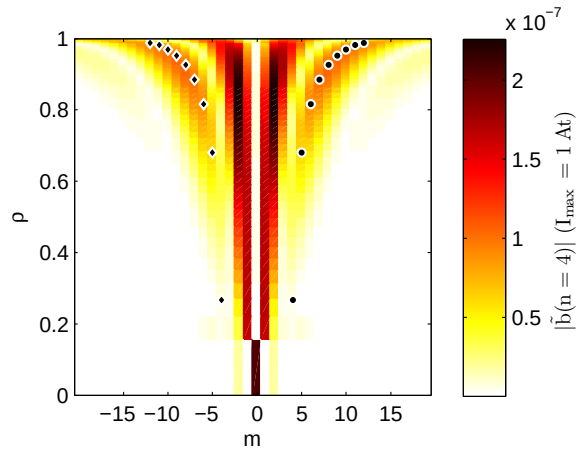

Figure 11. $\left|\tilde{b}(\rho, m, n = 4)\right|$. Target: $n_t = 4$ outside $\rho_{lim} = 0.911$. Optimized figure of merit r: $(w_e, w_g) = (0, 10^5)$. $I_{req} = 4.2\,\mathrm{kAt}$ and $r = 0.29$ (see figure 2).

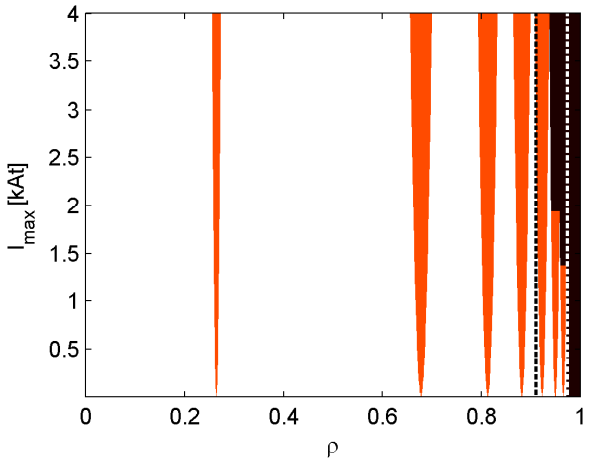

Figure 12. Ergodization map. Target: $n_t = 4$ outside $\rho_{lim} = 0.911$. Island width (red) and ergodic regions (dark brown) shown as a function of the maximal current fed in the SCS for the optimal figure of merit case. Vertical black dashed line: inner limit of the required ergodic zone according to the $\rho_{lim} = 0.911$ limit. Vertical white dashed line: $\psi_{01} = 0.95$.

decreasing the height of each row, both options leading to technical difficulties related to the increased current consumption and the higher number of feedthroughs.

Experimental application of the method developed here rises the question of the robustness of an optimal current distribution with respect to a change in the magnetic equilibrium, for example a variation of q_{95}. This question is addressed here by taking a reference equilibrium, $q_{95} = 4.1$, calculating its optimal relative current distribution $\{I_c\}_{q_{95}=4.1}$ and applying this distribution to the other equilibria in order to evaluate its figure of merit and required current. The results are displayed in figures 13 and 14 (dashed dotted lines). Figure 13 shows that the optimum is stable for $n_t = 2$ and $n_t = 3$,

but only asymmetrically stable for $n_t = 4$. This asymmetry appears because at $q_{95} = 4.1$, the q profile is aligned with the edge of a spectral ridge for $n_t = 4$. Experimentally, the variation of I_{req}, also present for the optimal current distributions case, might be another source of difficulties. Both observations suggest that the whole space of possible equilibria should be explored similarly to what has been done above before the experiments in order to assess the robustness of the chosen current distribution and the overall required current. Real time control of the coil currents would therefore have to rely on equilibrium recognition and precalculated sets of optimal currents.

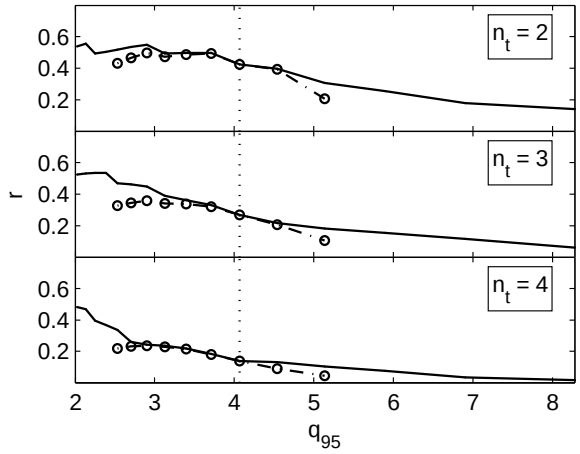

Figure 13. Solid lines (——): optimal figure of merit r_{opt} as a function of the safety factor q_{95} for targets $n_t = 2$, $n_t = 3$ and $n_t = 4$. Dashed-dotted lines (— · —○): $r(q_{95})$ calculated for a constant relative current distribution $\{I_c\}_{q_{95}=4.1}$, the current distribution optimizing r at $q_{95} = 4.1$ (vertical dotted line).

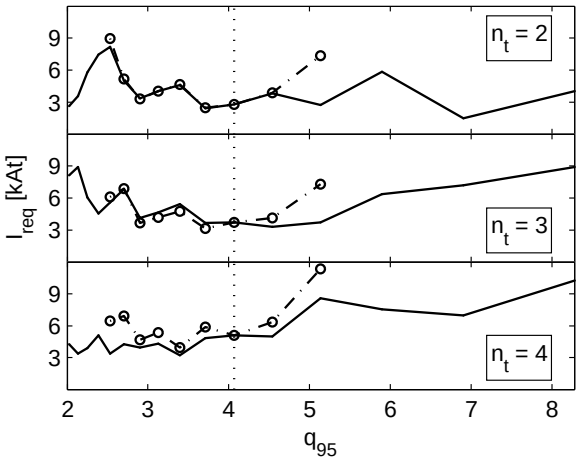

Figure 14. Solid lines (——): required current I_{req} as a function of the safety factor q_{95} for optimal figures of merit in the cases $n_t = 2$, $n_t = 3$ and $n_t = 4$. Dashed-dotted lines (— · —○): $I_{req}(q_{95})$ calculated for a constant relative current distribution $\{I_c\}_{q_{95}=4.1}$, the current distribution optimizing r at $q_{95} = 4.1$ (vertical dotted line).

3. Coil system characterization

This section develops the aspect of the spectral characterization of a coil system. The questions of spectral degeneracy, number of simultaneously controllable target modes, availability of optimization and efficiency in each toroidal mode are addressed.

3.1. General coil system

The most general approach to characterize a coil system consists in grouping coils in sets s of equivalent coils (e.g. identical coils on the same row, with arbitrary toroidal spacing) and using the first coil of the set to obtain the spectrum for the whole set:

$$\tilde{b}(\rho, m, n) = \sum_s \sum_c \tilde{b}^s_c(\rho, m, n) I^s_c = \sum_s \tilde{b}^s_0(\rho, m, n) \hat{I}^s(n) \tag{23}$$

$$\hat{I}^s(n) = \sum_c I^s_c \mathrm{e}^{-\mathrm{i}n\phi^s_c} \tag{24}$$

with ϕ^s_c the toroidal shift between the coils of the set s and $\hat{I}^s$ the **generalised discrete Fourier transform** of I^s_c in the current space (ϕ^s_c does not necessarily describe a regular grid). From equation (23), it follows that only one target mode can be given per set of equivalent coils per value of n. This is a determining argument in the question of allocation of the degrees of freedom related to the independent powering of the coils. Note that a row of coils could contain different sets, so that the "one mode per row" statement is not general.

3.2. Evenly-spaced coil system

In the case of evenly spaced coils, $\phi^s_c = (2\pi/N_s)c$, $c \in \{0, N_s - 1\}$ without necessarily being complete, degeneracy of modes occur:

$$\hat{I}^s(n + pN_s) = \hat{I}^s(n) \qquad \forall p \in \mathbb{N} \tag{25}$$

$$\hat{I}^s(N_s - n) = \hat{I}^{s*}(n) \tag{26}$$

In that case, only non degenerate target modes can be set simultaneously for each coil set. In addition, $\Im\left(\hat{I}^s(n \in \{N_s/2, N_s\})\right) = 0$, therefore limiting arbitrary phase setting of target modes in these cases.

3.3. Complete evenly-spaced coil system

Finally, in the case of complete evenly-spaced coil sets, $\hat{I}^s$ is equal to the standard discrete Fourier transform of I^s_c, so that modes in different values of n can be orthogonally activated by using Fourier modes for the currents in each coil row. The feature of orthogonal activation in even geometries implies the necessity to use a cross-mode cost function in the implementation of the Lagrange method, such as the cost based on the current amplitude. In the linear approach, the norm of the current vector is used. As it is proportional to $\sum_{s,n} |\hat{I}^s(n)|^2$ (the Fourier transform conserves the norm),

it is independent of the phase of the current modes. On the contrary, when using the non linear cost, based on the maximum of the current, an optimization of this phase is achieved, generally leading to a localization of the extrema of the current mode in the middle of two consecutive coils (see figure 4). If the gain due to a coil set is defined by:

$$g^s(n) = \frac{|\hat{I}^s(n)|}{\max_c(|I_c^s|)} \tag{27}$$

such an optimization can lead to a gain $g(2) = 5.6$ instead of the expected $g(2) = 4$, i.e. an increase of 40% of the mode amplitude for $n_t = 2$, in the TCV SCS case.

3.4. Loss of a coil in an evenly-spaced coil system

The loss of a coil in an evenly spaced coil system is of interest in terms of impact on the mode spectrum control. From the theory above, the main impact of such a loss is the loss of the orthogonal activation of modes. In terms of control, this loss can be compensated by adding a cost function on the side-bands that must be avoided. The latter cannot be avoided for the classes $n = 0$ and $n = N_s/2$ however.

It might be useful to note from (24) that for a single set of coils, whichever their toroidal spacing, the activation of the different toroidal modes only depends on $\hat{I}^s(n)$, which is independent of the plasma parameters. This feature can be used to reduce the number of parameters for the optimization, for example if fast calculation is required. For each value of n, one or two current basis vectors can be found and then used in the optimization algorithm. Of course, for complete sets of evenly spaced coils, these vectors are made of sine and cosine components. For the other cases, a Lagrange method can be used to find the basis vectors that minimize coupling with other values of n while assuring that their generalized Fourier transforms are orthogonal. Mathematically, if n_t is the toroidal mode number of the target mode, the cost function is written:

$$f = \sum_{n \neq n_t} \left| \hat{I}^s(n) \right|^2 \tag{28}$$

and the target $\hat{I}^s(n_t) = a_t \exp(\alpha_t)$. The α_t leading to the lowest cost is then selected, giving $\alpha_{t,1}$. This yields the first basis vector. The second basis vector is given by the same process but imposing $\alpha_{t,2} = \alpha_{t,1} + \pi/2$. The case of 1 coil missing out of a row of 8 coils is taken as an example. The generalized spectra of both basis vectors are shown in figure 15 for the case $n_t = 2$. As expected, the first vector is totally decoupled, since the phase is automatically adjusted to require a null current on the missing coil position. The drawback is that the gain is reduced to 4. The second vector, whose phase is adjusted to force orthogonality in Fourier space, is strongly coupled to the other modes.

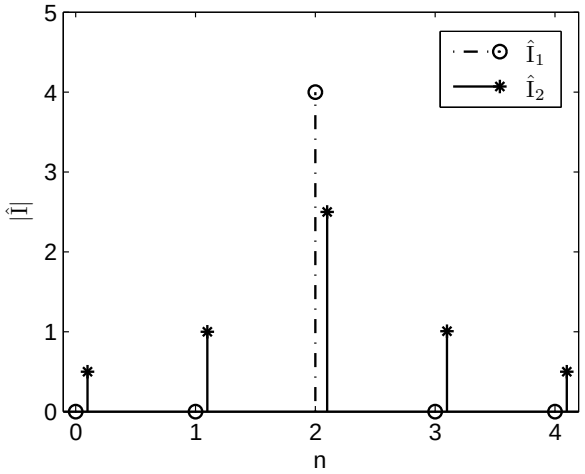

Figure 15. Generalized spectra of coil currents for one row of 8 coils where 1 coil is missing. The current distribution is optimal for $n_t = 2$, according to the method described in section 3.4.

4. Comments on the RMP coil set project for TCV

4.1. Choice of coil system geometry

In TCV, a saddle shape has been chosen for the coils. This maximizes the amplitude of the magnetic field created by the coil, for a given space occupation.

The coil array must be located on the low field side of the Tokamak to take advantage of the steeper pitch angle of the equilibrium magnetic field lines there. As a consequence much higher values of m are reached when analysing the perturbation in straight field line coordinates. The higher value of $\|\nabla\rho\|$ and the lower value of $B_{0,\phi}$ on the low field side also contribute to the maximization of b (see equation (3)). A comprehensive description of this aspect is given in [21].

The number of coil rows is determined as a trade-off between current requirements and spectrum shaping. A higher number of rows allow more control on modes with high values of m, but comes with smaller coils requiring more current. The number of coils in the toroidal direction defines the higher controllable value of n. Again, a trade-off between current requirements and coil system features must be chosen. Important aspects in this matter are the number of feedthroughs available, the cost of power supplies and the natural geometry of the Tokamak. In TCV, the portholes geometry, approximately 3 rows of 16 portholes, the maximal length allowed for each coil due to installation restriction and the flexibility in plasma positioning have driven the coil system design. The choice of having 8 rather than 4 coils per row has also been based on the larger variety of possible physical investigations that it allows.

4.2. Characterization

The considerations made in section 3 allow a characterization of the spectral features of the TCV SCS: 5 orthogonal classes of n are available ($n \in \{0, 1, 2, 3, 4\}$), with main degenerate pairs $\{0, 8\}$, $\{1, 7\}$, $\{2, 6\}$ and $\{3, 5\}$. For classes 1, 2 and 3, the 3 coil rows allow a maximum of 3 simultaneous targets per class (without simultaneous spectrum optimization), while for classes 0 and 4, only 1 target per class is allowed (with simultaneous spectrum optimization). The toroidal periodicity results in maximal gains for each row as follows: $g_{0,4} = 8$, $g_{1,3} = 4.3$ and $g_2 = 5.6$. For class 3, the degeneracy between $n = 3$ and $n = 5$ and the small spectral distance between these modes implies a non negligible effect of $n = 5$ modes when working in $n_t = 3$ configurations. Figure 16 shows how the small islands created by the $n = 5$ component of the perturbation overlap with the larger $n = 3$ islands and ergodize them.

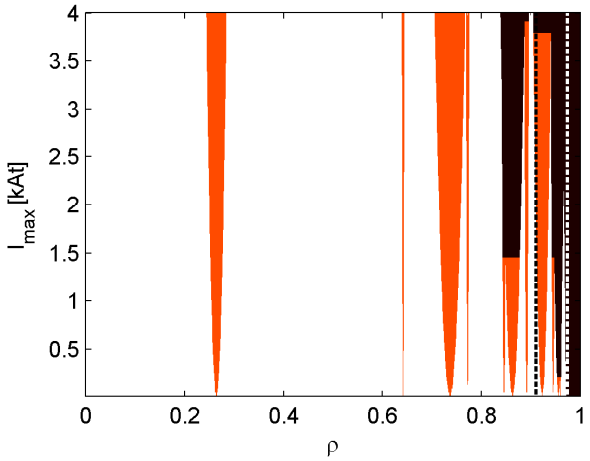

Figure 16. Ergodization map. Target: $n_t = 3$ outside $\rho_{lim} = 0.911$. Island width (red) and ergodic regions (dark brown) shown as a function of the maximal current fed in the SCS for the optimal figure of merit case. Vertical black dashed line: inner limit of the required ergodic zone according to the $\rho_{lim} = 0.911$ limit. Vertical white dashed line: $\psi_{01} = 0.95$. The small islands are due to the $n = 5$ degenerate component.

5. Conclusion

A comprehensive study of RMP calculation and optimization, based on vacuum perturbation field and independent powering of the coils, has been presented. The efficiency of the method has been proven on a number of experimentally relevant cases: $n = 2$, $n = 3$ and $n = 4$ targets for a typical H-mode plasma. A general procedure for spectral characterization of coil systems has been developed and its application to common special cases detailed. This work could be applied to any existing coil system, with a special dedicated application to the SCS proposed for ASDEX [25] since two different subsets of coils are planned for the midplane row.

The TCV SCS and its design physical basis have been briefly presented. A subsequent dedicated publication will follow.

Acknowledgments

The authors are grateful to Eric Nardon and Yunfeng Liang for valuable discussions. This work was supported in part by the Swiss National Science Foundation.

References

[1] A. Fasoli. Overview of physics research on the TCV Tokamak. *22nd IAEA Fusion Energy Conference, Geneva*, OV, 1–1. IAEA, October 2008.

[2] G. T. A. Huysmans. ELMs: MHD instabilities at the transport barrier. *Plasma Physics and Controlled Fusion*, 47(12B):B165–B178, 2005.

[3] Y. R. Martin *et al.* Accessibility and properties of ELMy H-mode and ITB plasmas in TCV. *Plasma Physics and Controlled Fusion*, 45(12 A), 2003.

[4] G. Federici A. Loarte and G. Strohmayer. Assessment of erosion of the ITER divertor targets during type I ELMs. *Plasma Physics and Controlled Fusion*, 45(9):1523–1547, 2003.

[5] R.J. Hawryluk *et al.* Principal physics developments evaluated in the iter design review. *Nuclear Fusion*, 49(6), 2009.

[6] K. H. Burrell and T. E. Evans. ELM suppression in low edge collisionality H-mode discharges using n = 3 magnetic perturbations. *Plasma Physics and Controlled Fusion*, 47(12B):B37–B52, 2005.

[7] T. E. Evans and R. A. Moyer. Suppression of large edge localized modes with edge resonant magnetic fields in high confinement DIII-D plasmas. *Nuclear Fusion*, 45(7):595–607, 2005.

[8] Y. Liang *et al.* Active control of type-I edge-localized modes with n=1 perturbation fields in the JET Tokamak. *Physical Review Letters*, 98(26), 2007.

[9] S. J. Fielding, R. J. Buttery, A. R. Field, P. B. Jones, H. Meyer, M. Valovic, and H. R. Wilson. ELM control in COMPASS-D. In *28th EPS Conference on Controlled Fusion and Plasma Physics, Funchal*, volume 25A, pages 1825 – 1828, June 2001.

[10] D. A. Gates *et al.* Overview of results from the national spherical torus experiment. In *22nd IAEA Fusion Energy Conference, Geneva*, volume OV, pages 3–1. IAEA, October 2008.

[11] H. Meyer *et al.* Overview of physics results from mast. *Nuclear Fusion*, 49(10), 2009.

[12] E. Nardon *et al.* ELM control by resonant magnetic perturbations on JET and MAST. *Journal of Nuclear Materials*, 390-391:773 – 776, 2009. Proceedings of the 18th International Conference on Plasma-Surface Interactions in Controlled Fusion Device.

[13] M.J. Schaffer J.E. Menard M.P. Aldan J.M. Bialek T.E. Evans and R.A. Moyer. Study of in-vessel nonaxisymmetric elm suppression coil concepts for iter. *Nuclear Fusion*, 48(2), 2008.

[14] M. Bécoulet *et al.* Numerical study of the resonant magnetic perturbations for type i edge localized modes control in iter. *Nuclear Fusion*, 48(2), 2008.

[15] A.M. Garofalo *et al.* Observation of plasma rotation driven by static nonaxisymmetric magnetic fields in a Tokamak. *Physical Review Letters*, 101(19), 2008.

[16] M. Bécoulet *et al.* Physics of penetration of resonant magnetic perturbations used for type i edge localized modes suppression in Tokamaks. *Nuclear Fusion*, 49(8), 2009.

[17] K.C. Shaing S.A. Sabbagh M.S. Chu M. Becoulet and P. Cahyna. Effects of orbit squeezing on neoclassical toroidal plasma viscosity in Tokamaks. *Physics of Plasmas*, 15(8), 2008.

[18] S. M. Wolfe *et al.* Nonaxisymmetric field effects on alcator C-Mod. *Physics of Plasmas*, 12(5):1–10, 2005.

[19] J. D. Hanson. Correcting small magnetic field non-axisymmetries. *Nuclear Fusion*, 34(3):441–448, 1994.

[20] J. D. Hanson. Using external coils to correct field errors in Tokamaks. *Plasma Science, IEEE Transactions on*, 27(6):1588–1595, Dec 1999.

[21] P. Cahyna, R. Panek, V. Fuchs, L. Krlin, M. Becoulet, G. Huysmans and E. Nardon. The optimization of resonant magnetic perturbation spectra for the COMPASS Tokamak. *Nuclear Fusion*, 49(5):055024 (7pp), 2009.

[22] J.-M. Moret. A software package to manipulate space dependencies and geometry in magnetic confinement fusion. *Review of Scientific Instruments*, 76(7):073507, 2005.

[23] M. E. Fenstermacher *et al.* Effect of island overlap on edge localized mode suppression by resonant magnetic perturbations in diii-d. *Physics of Plasmas*, 15(5):056122, 2008.

[24] F. Hofmann. FBT - a free-boundary Tokamak equilibrium code for highly elongated and shaped plasmas. *Computer Physics Communications*, 48(2):207 – 221, 1988.

[25] W. Suttrop *et al.* In-vessel saddle coils for MHD control in ASDEX upgrade. *Fusion Engineering and Design*, 84(2-6):290 – 294, 2009. Proceeding of the 25th Symposium on Fusion Technology - (SOFT-25).